PHYSICAL REVIEW D **83,** 114004 (2011)

Exclusive production of ω meson in proton-proton collisions at high energies

Anna Cisek,[1,*] Piotr Lebiedowicz,[1,†] Wolfgang Schäfer,[1,‡] and Antoni Szczurek[1,2,§]

[1]*Institute of Nuclear Physics PAN, PL-31-342 Cracow, Poland*

[2]*University of Rzeszów, PL-35-959 Rzeszów, Poland*

(Received 31 January 2011; published 1 June 2011)

First we calculate cross section for the $\gamma p \to \omega p$ reaction from the threshold to very large energies. At low energies the pion exchange is the dominant mechanism. At large energies the experimental cross section can be well described assuming Pomeron exchange within the k_t-factorization approach by adjusting light quark constituent mass. Next we calculate differential distributions for the $pp \to pp\omega$ reaction at RHIC, Tevatron and LHC energies for the first time in the literature. We consider photon-Pomeron (Pomeron-photon), photon-pion (pion-photon) as well as novel diffractive hadronic bremsstrahlung mechanisms. The latter are included in the meson/Reggeon exchange picture with parameters fixed from the known phenomenology. Interesting rapidity distributions are predicted. The hadronic bremsstrahlung contributions dominate at large (forward, backward) rapidities. At small energies the photon-Pomeron contribution is negligible compared to the bremsstrahlung contributions. It could be, however, easily identified at large energies at midrapidities. Absorptions effects are included and discussed. Our predictions are ready for verification at RHIC and LHC.

DOI: 10.1103/PhysRevD.83.114004 PACS numbers: 13.60.Le, 12.40.Nn, 13.85.−t, 14.40.Be

I. INTRODUCTION

The mechanism of exclusive production of mesons in hadron-hadron collisions at high energies became recently a very active field of research (see [1] and references therein). The recent works concentrated on the production of χ_c mesons (see e.g. [2]) where the QCD mechanism is similar to the exclusive production of the Higgs boson. The latter process is an alternative to the inclusive production of the Higgs boson.

The (virtual) photoproduction of vector mesons in $\gamma^* p$ collisions is also a vivid and active field of research. Here the main interest was related to the wealth of experimental data obtained by the H1 and ZEUS Collaborations at the HERA collider. For a review of the experimental and theoretical status until 2006, see [3]. The subject continues to be actively researched also in recent years. The focus being e.g. on saturation phenomena in the small-x gluon distribution [4], on models based on the general principles of Regge theory [5], as well as on investigations of systematic treatment of higher twist contributions in the high Q^2 limit [6].

The exclusive photoproduction of vector mesons can also be studied in hadron-hadron collisions [7]. Here the dominant mechanism is photon-Pomeron (Pomeron-photon) fusion which for heavy vector quarkonia (J/Ψ, Υ) probes the proton's gluon density at small x (see e.g. [8,9]). Recently also the quasidiffractive large-t, large rapidity gap photoproduction of vector mesons in hadronic collisions has attracted some interest, see e.g. [10,11]; the latter calculation using a theoretical framework which was developed in [12].

What these works have in common is that they involve a hard scale of some sort—either the large mass of a heavy quark, or a large momentum transfer. The soft mechanism of exclusive light vector meson production in proton-proton collisions was almost not studied in the literature, a recent exception is the ϕ meson [13].

Here we will show that exclusive production of ω mesons in proton-proton collisions is very different than similar processes for ϕ [13], J/Ψ [8] or Υ [9]. Before this process was studied only close to its production threshold. Various theoretical models (see Refs. [14–18]) were developed to describe the lower-energy data [19]. Here the dominant mechanisms are meson exchange processes as well as the ω-meson bremsstrahlung driven by meson exchanges. How the situation changes at high energy is interesting but has not been studied so far. While at low energy the meson exchanges (π, ρ, ω, σ) are the driving t-channel exchanges for the ω bremsstrahlung, at high energy their role is taken over by the Pomeron exchange. The latter will be treated here purely phenomenologically. A similar hadronic bremsstrahlung-type mechanism is the Deck-mechanism for diffractive production of πN final states in pp collisions [20], for a review, see e.g. [21].

In the present paper we intend to make predictions for being in operation colliders RHIC, Tevatron and LHC. The hadronic bremsstrahlung mechanisms are expected to be enhanced for exclusive production of ω meson compared to other vector mesons as the $g_{\omega NN}$ coupling constant is known to be large from low energy phenomenology [18,22]. We will also show how important the photoproduction mechanisms are, as discussed previously in the context of exclusive heavy vector quarkonium production [8,9].

*anna.cisek@ifj.edu.pl
†piotr.lebiedowicz@ifj.edu.pl
‡wolfgang.schafer@ifj.edu.pl
§antoni.szczurek@ifj.edu.pl

At this point it is interesting to remember that the exclusive production of vector mesons at high energies has been proposed as a promising channel for a discovery/study of the Odderon [23,24]. This fact is simply related to the odd C parity of the vector meson. It now turns out, that for the previously studied exclusive J/Ψ and Υ production, the main competitor to the Odderon-Pomeron fusion mechanism exchange is the photoproduction mechanism.

In this regard it is important to stress that the unique hadronic bremsstrahlung mechanism active in exclusive ω production precludes an interpretation of a possible excess over photoproduction in terms of an Odderon. Indeed, as will be shown below, the strong coupling of the ω to protons entails a surprisingly large cross section for central ω production at high energies. This is despite the fact that formally the t-channel exchange of ω's is decreasing with the size of the rapidity gap in comparison to the Odderon.

In this context we mention that it has also been proposed to search for the Odderon in the photoproduction of C-even pion pairs. Their interference with the Pomeron-produced C-odd pions will lead to characteristic angular asymmetries [25] (for the case of large photon virtualities, see [26]). While in principle photoproduction of continuum pion pairs is just as well possible as the production of vector meson resonances studied here, the relevant asymmetries will be heavily diluted by the C-even pion pairs produced from Pomeron-Pomeron fusion (for a recent study of the latter mechanism, see [27]).

II. PHOTOPRODUCTION MECHANISM FOR $\gamma p \to \omega p$

A. Pomeron exchange

Let us concentrate on the $\gamma p \to \omega p$ reaction which is a building block for the $pp \to pp\omega$ reaction. Photoproduction of the vector meson in photon-proton collisions is very interesting from both experimental and theoretical side. The corresponding cross sections have been measured by the ZEUS Collaboration at HERA at virtuality of photon $Q^2 \simeq 0$ GeV^2 for ω photoproduction [28] and at large values Q^2 for ω electroproduction $ep \to e\omega p$ [29]. The amplitude for this reaction is shown schematically in Fig. 1. The Pomeron exchange is modeled by a pQCD gluon ladder. The details for how to calculate the amplitude are explained in Refs. [3,9]. The following representation for the imaginary part of the amplitude for the transverse polarization for forward photoproduction $\gamma p \to \omega p$ process is used:

$$\begin{aligned}&\mathrm{Im}\mathcal{M}(W, \Delta^2 = 0, Q^2 = 0)\\ &= W^2 \frac{c_V\sqrt{4\pi\alpha_{\mathrm{em}}}}{4\pi^2} \int dz d^2\boldsymbol{k} d^2\boldsymbol{\kappa} \psi_V(z, \boldsymbol{k}^2)\\ &\quad \times \mathcal{F}(x_{\mathrm{eff}}, \boldsymbol{\kappa}^2) I(z, \boldsymbol{k}, \boldsymbol{\kappa}),\end{aligned} \tag{2.1}$$

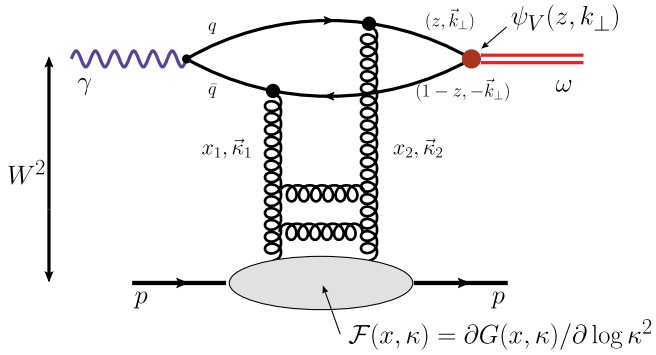

FIG. 1 (color online). A sketch of the amplitude for exclusive photoproduction $\gamma p \to \omega p$ process. In addition, some kinematical variables are shown.

where the precise form of the function $I(z, \boldsymbol{k}, \boldsymbol{\kappa})$ derives from the quark loop in Fig. 1 and can be found in [3]. Here $\mathcal{F}(x_{\mathrm{eff}}, \boldsymbol{\kappa}^2)$ is an unintegrated gluon distribution, taken from [30], which following [3] is evaluated at $x_{\mathrm{eff}} = c_{\mathrm{skewed}}(m_\omega^2/W^2)$. Notice that this particular unintegrated glue also incorporates the region of soft gluon transverse momenta $\boldsymbol{\kappa}$, where it can be viewed as a model of the soft Pomeron in terms of nonperturbative gluons. The process at hand is sensitive to this domain of soft momenta. The charge-isospin factor c_V is $c_\omega = 1/\sqrt{2}(e_u + e_d) = 1/(3\sqrt{2})$.

The full amplitude for the $\gamma p \to \omega p$ process at finite momentum transfer is given as

$$\begin{aligned}&\mathcal{M}(W, \Delta^2, Q^2 = 0)\\ &= (i + \rho)\,\mathrm{Im}\mathcal{M}(W, \Delta^2 = 0, Q^2 = 0) \exp\left(\frac{-B(W)\Delta^2}{2}\right),\end{aligned} \tag{2.2}$$

where ρ is a ratio of real to imaginary part of the amplitude and $B(W)$ is the slope parameter dependent on the photon-proton center-of-mass energy and is parametrized as

$$B(W) = B_0 + 2\alpha'_{\mathrm{eff}} \ln\left(\frac{W^2}{W_0^2}\right), \tag{2.3}$$

with $W_0 = 95$ GeV, $B_0 = 11$ GeV^{-2}, and $\alpha'_{\mathrm{eff}} = 0.25$ GeV^{-2} [31].

Our amplitude is normalized to the total cross section:

$$\sigma(\gamma p \to \omega p) = \frac{1 + \rho^2}{16\pi B(W)} \left| \mathrm{Im}\frac{\mathcal{M}(W, \Delta^2 = 0, Q^2 = 0)}{W^2} \right|^2. \tag{2.4}$$

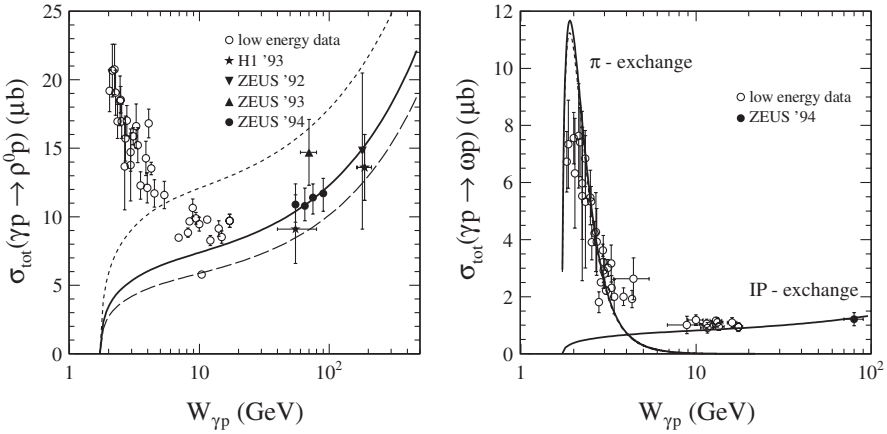

FIG. 2. Total cross section for the photoproduction $\gamma p \to \rho^0 p$ (left panel) and $\gamma p \to \omega p$ (right panel) processes as a function of the photon-proton center-of-mass energy. In the calculation of the $\mathbb{P}$-exchange mechanism the Gaussian wave function of the ρ^0 and ω mesons is used. At low energies π-exchange is the dominant mechanism. The curves are described in the text. Our results are compared with the HERA data [28,48–51] (solid marks) and with a compilation of low energy data [52,53] (open circles).

The radial light cone wave function of the vector meson can be regarded as a function of three-momentum $\boldsymbol{p} = (\vec{p}, p_z)$, where $\vec{p} = \vec{k}$, $p_z = (2z-1)M/2$, and then

$$\psi_V(z,\vec{k}^2) \to \psi_V(p^2), \quad \frac{dz d^2\vec{k}}{z(1-z)} \to \frac{4d^3\boldsymbol{p}}{M}, \quad p^2 = \frac{M^2 - 4m_q^2}{4}. \tag{2.5}$$

Following [3], in our calculation we use a Gaussian wave function, representing a standard harmonic-oscillator type quark model, which turned out to be superior over a Coulomb wave function (which a power-law tail in momentum space) for J/Ψ, Υ and ϕ mesons exclusive photoproduction [8,9,13]

$$\psi_V(p^2) = N \exp\left(-\frac{p^2 a_1^2}{2}\right). \tag{2.6}$$

The parameter a_1 is obtained by fitting to the electronic decay width

$$\Gamma(V \to e^+e^-) = \frac{4\pi\alpha_{\rm em}^2 c_V^2}{3m_\omega^3} \cdot g_V^2, \tag{2.7}$$

where $\Gamma(\omega \to e^+e^-) = 0.6$ keV [32] and imposing the normalization condition

$$1 = \frac{N_c 4\pi}{(2\pi)^3} \int_0^\infty p^2 dp 4M \psi_V^2(p^2). \tag{2.8}$$

In our calculation we use leading-order approximation, i.e. we neglect a possible NLO K factor. The parameter g_V can be expressed in terms of the ω-meson wave function as [3]

$$g_V = \frac{8N_c}{3} \int \frac{d^3\vec{p}}{(2\pi)^3} (M + m_q)\psi_V(p^2). \tag{2.9}$$

Having in view theoretical uncertainties in defining light quark mass it is treated here as a model parameter. In Fig. 2 we show the total cross section for the exclusive $\gamma p \to \rho^0 p$ (left panel) and $\gamma p \to \omega p$ (right panel) processes as a function of the γp center-of-mass energy $W_{\gamma p}$ for the photon virtuality $Q^2 = 0$ GeV^2. Our results for exclusive ρ^0 and ω mesons production are compared with the corresponding experimental data. For the ρ^0 meson we present results for three different values of the u and d quark masses assumed here to be identical. The dashed line (bottom) is for $m_q = 0.33$ GeV, the dotted line (top) for $m_q = 0.22$ GeV and the thick solid line (fitted to experimental data) for $m_q = 0.3$ GeV. Because the results for $m_q = 0.3$ GeV give the best description of experimental data, this mass will be used in further calculations. In calculation the Gaussian wave function is used. We see that it gives quite a good description of the high energy ω-meson data. At low energies the pion exchange mechanism dominates [33,34]. This will be discussed in the following subsection.

B. Pion exchange

The amplitude for the π-exchange shown in Fig. 3 can be written as

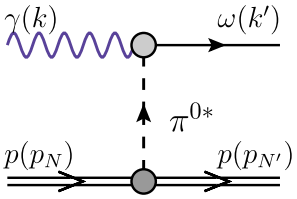

FIG. 3 (color online). Diagram with the π-exchange for exclusive photoproduction $\gamma p \to \omega p$.

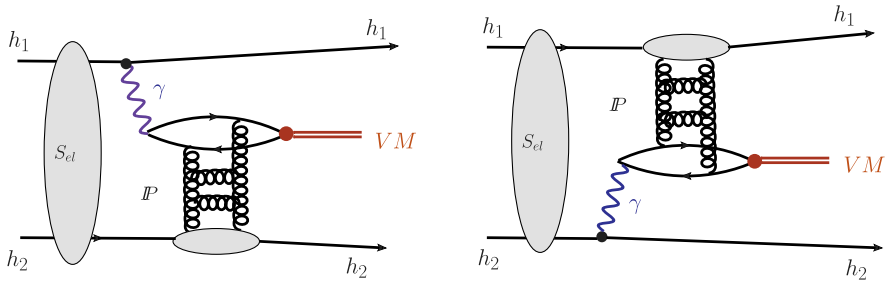

FIG. 4 (color online). A sketch of the exclusive photoproduction $pp \to pp\omega$ amplitudes with absorptive corrections.

$$\mathcal{M}^{\pi^0-\text{exch.}}_{\lambda_\gamma,\lambda_N\to\lambda_\omega,\lambda_{N'}} = g_{\omega\pi^0\gamma}F_{\omega\pi\gamma}(t)\varepsilon^{\beta\mu\nu\lambda}k_\mu k'_\nu\varepsilon_\beta(k,\lambda_\gamma)\varepsilon^*_\lambda(k',\lambda_\omega) \times g_{\pi^0NN}F_{\pi NN}(t)\frac{1}{t-m_\pi^2}\bar{u}(p_{N'},\lambda_{N'})i\gamma_5 u(p_N,\lambda_N). \tag{2.10}$$

The $g_{\omega\pi^0\gamma}$ coupling constant in the formula above is obtained from the ω partial decay width through the relation

$$\Gamma(\omega\to\pi^0\gamma) = \mathcal{BR}(\omega\to\pi^0\gamma)\cdot\Gamma_{\text{tot}} = \frac{g^2_{\omega\pi^0\gamma}}{96\pi}\cdot m_\omega^3\left(1-\frac{m_\pi^2}{m_\omega^2}\right)^3. \tag{2.11}$$

Taking experimental partial decay width $\Gamma(\omega\to\pi^0\gamma)$ from [32] we get $g_{\omega\pi^0\gamma}\approx 0.7\ \text{GeV}^{-1}$ which is consistent with the values used in Refs. [34,35].[1] The pion-nucleon coupling constant $g_{\pi NN}$ is relatively well known [36]. In our calculations the coupling constant is $g^2_{\pi NN}/4\pi = 13.5$, and $\varepsilon_\beta(k,\lambda_\gamma)$ and $\varepsilon^*_\lambda(k',\lambda_\omega)$ are the polarization vectors of the photon and ω meson, respectively.

We describe the low energy data shown in Fig. 2 (right panel) with $\Lambda_{\text{mon}}\approx 0.7$ GeV for the monopole form factors by the dashed line:

$$F(t) = \frac{\Lambda^2_{\text{mon}}-m_\pi^2}{\Lambda^2_{\text{mon}}-t} \tag{2.12}$$

or with $\Lambda_{\text{exp}}\approx 0.8$ GeV for the exponential form factors by the solid line:

$$F(t) = \exp\left(\frac{t-m_\pi^2}{\Lambda^2_{\text{exp}}}\right). \tag{2.13}$$

The cutoff parameters obtained from the fit are significantly smaller than e.g. those used in the Bonn model [22]. Such soft form factors may be due to active coupling with the πN and ρN channels not included explicitly here nor in the literature. The pion exchange describes only angular distributions at forward angles. At larger angles there are other mechanisms as nucleon exchanges or s-channel nucleon resonances [34,37]. A more refined analysis in the peak region would require a description of new, very precise CLAS Collaboration data [38] for full range angular distributions. Such an analysis would need to also include channel couplings discussed above.

The form factors found here will be used when discussing $\gamma\pi^0$ and $\pi^0\gamma$ exchanges in the $pp\to pp\omega$ reaction.

[1]Please note different normalization convention of the coupling constant in all the papers.

III. THE AMPLITUDES FOR THE $pp \to pp\omega$ REACTION

A. $\gamma\mathbb{P}$ and $\mathbb{P}\gamma$ exchanges

The diagrams for the pp and $p\bar{p}$ collisions in Fig. 4 show schematically the amplitudes for photon-Pomeron (Pomeron-photon) exchanges with absorptive correction, including elastic rescattering. The full amplitude (with absorptive correction) for the $pp\to pp\omega$ or $p\bar{p}\to p\bar{p}\omega$ reactions can be written as

$$\boldsymbol{M}(\vec{p}_1,\vec{p}_2) = \int\frac{d^2\vec{k}}{(2\pi)^2}S_{el}(\vec{k})\boldsymbol{M}^{(0)}(\vec{p}_1-\vec{k},\vec{p}_2+\vec{k}) = \boldsymbol{M}^{(0)}(\vec{p}_1,\vec{p}_2) - \delta\boldsymbol{M}(\vec{p}_1,\vec{p}_2), \tag{3.1}$$

where

$$S_{el}(\vec{k}) = (2\pi)^2\delta^{(2)}(\vec{k}) - \frac{1}{2}T(\vec{k}), \qquad T(\vec{k}) = \sigma^{pp}_{\text{tot}}(s)\exp\left(-\frac{1}{2}B_{el}\vec{k}^2\right). \tag{3.2}$$

Here $\vec{p}_1$ and $\vec{p}_2$ are the transverse momenta of outgoing protons (RHIC, LHC) or proton and antiproton (Tevatron). In practical evaluations we take $B_{el} = 14\ \text{GeV}^{-2}$, $\sigma^{pp}_{\text{tot}} = 52$ mb for the RHIC energy $W = 200$ GeV, $B_{el} = 17\ \text{GeV}^{-2}$, $\sigma^{p\bar{p}}_{\text{tot}} = 76$ mb [39] for the Tevatron energy $W = 1.96$ TeV and $B_{el} = 21\ \text{GeV}^{-2}$, $\sigma^{pp}_{\text{tot}} = 100$ mb for the LHC energy $W = 14$ TeV.

The Born-amplitude (without absorptive correction) can be written in the form of a two-dimensional vector (corresponding to the two transverse (linear) polarizations of the final state vector meson) [8] as

$$\boldsymbol{M}^{(0)}(\vec{p}_1,\vec{p}_2) = e_1\frac{2}{z_1}\frac{\vec{p}_1}{t_1}\mathcal{F}_{\lambda_1'\lambda_1}(\vec{p}_1,t_1)\mathcal{M}_{\gamma^* h_2\to Vh_2}(s_2,t_2,Q_1^2) + e_2\frac{2}{z_2}\frac{\vec{p}_2}{t_2}\mathcal{F}_{\lambda_2'\lambda_2}(\vec{p}_2,t_2)\mathcal{M}_{\gamma^* h_1\to Vh_1}(s_1,t_1,Q_2^2), \quad (3.3)$$

where $\mathcal{M}_{\gamma^* h_2\to Vh_2}(s_2,t_2,Q_1^2)$ and $\mathcal{M}_{\gamma^* h_1\to Vh_1}(s_1,t_1,Q_2^2)$ are the amplitudes for photoproduction discussed above (see (2.2)). Because of the presence of the Dirac electromagnetic form factor of the proton/antiproton only small Q_1^2 and Q_2^2 enter the amplitude for the hadronic process. This means that in practice one can put $Q_1^2 = Q_2^2 = 0\ \mathrm{GeV}^2$ for the $\gamma^* p\to Vp$ amplitudes. We used the assumption of s-channel helicity conservation in the $\gamma\to\omega$ transition, $\lambda_\gamma = \lambda_V$.

The absorptive correction for the amplitude have the form:

$$\delta\boldsymbol{M}(\vec{p}_1,\vec{p}_2) = \int\frac{d^2\vec{k}}{2(2\pi)^2}T(\vec{k})\boldsymbol{M}^{(0)}(\vec{p}_1-\vec{k},\vec{p}_2+\vec{k}). \quad (3.4)$$

The differential cross section is expressed in terms of the amplitude $\boldsymbol{M}$ as

$$d\sigma = \frac{1}{512\pi^4 s^2}|\boldsymbol{M}|^2 dy dt_1 dt_2 d\phi. \quad (3.5)$$

where y is rapidity of the ω meson, $t_{1,2}\simeq -\vec{p}_{1,2}^{\,2}$ and ϕ is the azimuthal angle between transverse momenta $\vec{p}_1$ and $\vec{p}_2$.[2]

B. $\gamma\pi^0$ and $\pi^0\gamma$ exchanges

As shown in Fig. 2 the QCD mechanism discussed in Sec. II A does not describe the huge close-to-threshold enhancement of the cross section. This indicates a presence of another mechanisms of omega photoproduction. Neutral pion exchange is the best candidate which describes the low energy data as discussed in Sec. II B. Therefore for the $pp\to pp\omega$ reaction we should also include photon-pion and pion-photon exchanges. The underlying mechanisms are shown in Fig. 5.

The amplitudes for the two new processes can be easily written as

$$\mathcal{M}^{\gamma\pi^0-\mathrm{exch.}}_{\lambda_a\lambda_b\to\lambda_1\lambda_2\lambda_3} = eF_1(t_1)\bar{u}(p_1,\lambda_1)\gamma^\alpha u(p_a,\lambda_a)\frac{-g_{\alpha\beta}}{t_1}g_{\omega\pi^0\gamma}F_{\gamma\pi\to\omega}(t_1,t_2) \times\varepsilon^{\beta\mu\nu\lambda}q_{1\mu}p_{3\nu}\varepsilon^*_\lambda(p_3,\lambda_3)g_{\pi^0 NN}F_{\pi NN}(t_2) \times\frac{1}{t_2-m_\pi^2}\bar{u}(p_2,\lambda_2)i\gamma_5 u(p_b,\lambda_b), \quad (3.6)$$

[2]In the following for brevity we shall use notation $t_{1,2}$ which means t_1 or t_2.

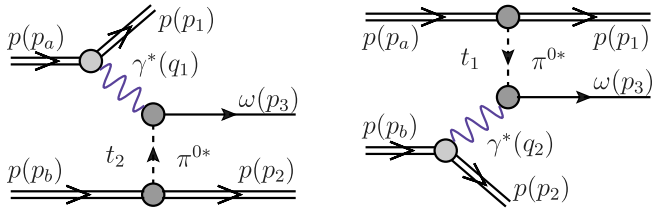

FIG. 5 (color online). Diagrams with the $\gamma\pi^0$ and $\pi^0\gamma$ exchange amplitudes in the $pp\to pp\omega$ reaction.

$$\mathcal{M}^{\pi^0\gamma-\mathrm{exch.}}_{\lambda_a\lambda_b\to\lambda_1\lambda_2\lambda_3} = g_{\pi^0 NN}F_{\pi NN}(t_1)\frac{1}{t_1-m_\pi^2}\bar{u}(p_1,\lambda_1)i\gamma_5 u(p_a,\lambda_a) \times\frac{-g_{\alpha\beta}}{t_2}g_{\omega\pi^0\gamma}F_{\gamma\pi\to\omega}(t_2,t_1)\varepsilon^{\beta\mu\nu\lambda}q_{2\mu}p_{3\nu}\varepsilon^*_\lambda(p_3,\lambda_3) \times eF_1(t_2)\bar{u}(p_2,\lambda_2)\gamma^\alpha u(p_b,\lambda_b), \quad (3.7)$$

where $F_1(t_{1,2})$ are the Dirac electromagnetic form factors of participating protons. The $g_{\omega\pi^0\gamma}$ constant was obtained from the omega partial decay width as discussed in Sec. II B. The coupling of the pion to the nucleon is described by the pion-nucleon coupling constant $g_{\pi NN}$ and the corresponding form factor is taken in the exponential form:

$$F_{\pi NN}(t_{1,2}) = \exp\left(\frac{t_{1,2}-m_\pi^2}{\Lambda^2_{\pi NN}}\right). \quad (3.8)$$

The central vertices involve off shell particles. Here the $\gamma\pi^0$ and $\pi^0\gamma$ form factors are taken in the following factorized form:

$$F_{\gamma\pi\to\omega}(t_1,t_2) = \frac{m_\rho^2}{m_\rho^2-t_1}\exp\left(\frac{t_2-m_\pi^2}{\Lambda^2_{\omega\pi\gamma}}\right). \quad (3.9)$$

The factor describing the virtual photon coupling is taken as in the vector dominance model. In practical calculations we take $\Lambda_{\pi NN} = 0.8$ GeV and $\Lambda_{\omega\pi\gamma} = 0.8$ GeV as found from the fit to the $\gamma p\to\omega p$ experimental data.

At high energies often light cone form factors are used instead of the t_1 or t_2 dependent ones discussed above (see Eq. (3.8)). In such an approach the pion is rather a constituent of the initial proton. Then the form factors are parametrized in terms of the squared invariant masses of the πN system:

$$M^2_{2,\pi N}(z_2,p_{2t}^2) = \frac{m_N^2+p_{2t}^2}{z_2}+\frac{m_\pi^2+p_{2t}^2}{1-z_2}, \qquad M^2_{1,\pi N}(z_1,p_{1t}^2) = \frac{m_N^2+p_{1t}^2}{z_1}+\frac{m_\pi^2+p_{1t}^2}{1-z_1}, \quad (3.10)$$

where the longitudinal momentum fractions of outgoing protons with respect to the initial protons can be calculated from energies and z components of momenta of participating protons

$$z_2 = (p_{20} - p_{2z})/(p_{b0} - p_{bz}),$$
$$z_1 = (p_{10} + p_{1z})/(p_{a0} + p_{az}). \tag{3.11}$$

The light cone form factors are parametrized then as

$$F_{\pi NN}(M^2_{2,\pi N}) = \exp\left(-\frac{M^2_{2,\pi N}(z_2, p^2_{2t}) - m^2_N}{2\Lambda^2_{\rm LC}}\right),$$
$$F_{\pi NN}(M^2_{1,\pi N}) = \exp\left(-\frac{M^2_{1,\pi N}(z_1, p^2_{1t}) - m^2_N}{2\Lambda^2_{\rm LC}}\right). \tag{3.12}$$

The parameter $\Lambda_{\rm LC}$ in the light cone parametrization was fitted in Ref. [40] to the data on forward nucleon production and the value $\Lambda_{\rm LC} = 1.1$ GeV was found.

The amplitude for processes shown in Fig. 5 is calculated numerically for each point in the phase space. In calculating the cross section we perform integration in $\log_{10}(p_{1t})$ (for $\gamma\pi$-exchange) and $\log_{10}(p_{2t})$ (for $\pi\gamma$-exchange) instead of in p_{1t} and p_{2t}.

IV. HADRONIC BREMSSTRAHLUNG MECHANISMS

A. The amplitude in the standard approach

The strong coupling of the ω meson to the nucleon causes the hadronic bremsstrahlung mechanisms to become important. The bremsstrahlung mechanisms for exclusive production of ω discussed here are shown schematically in Fig. 6. In the case of ω production the diagrams with intermediate nucleon resonances are negligible (see [32]). Because at high energy the Pomeron is the driving mechanism of bremsstrahlung, it is logical to call the mechanisms a diffractive bremsstrahlung to distinguish from the low energy bremsstrahlung driven by meson exchanges.

It is straightforward to evaluate the contribution of diagrams shown in Fig. 6. The Born amplitudes read

$$\mathcal{M}^{(a)}_{\lambda_a\lambda_b\to\lambda_1\lambda_2\lambda_3} = \bar{u}(p_1,\lambda_1)\varepsilon^*_\mu(p_3,\lambda_3)\gamma^\mu S_N(p^*_{1f})u(p_a,\lambda_a)g_{\omega NN}F_{\omega N^*N}(p^{*2}_{1f})F_{\mathbb{P}NN^*}(p^{*2}_{1f})$$
$$\times is_{ab}C^{NN}_{\mathbb{P}}\left(\frac{s_{ab}}{s_0}\right)^{\alpha_{\mathbb{P}}(t_2)-1}\exp\left(\frac{B^{NN}_{\mathbb{P}}t_2}{2}\right)\delta_{\lambda_2\lambda_b}, \tag{4.1}$$

$$\mathcal{M}^{(b)}_{\lambda_a\lambda_b\to\lambda_1\lambda_2\lambda_3} = \bar{u}(p_2,\lambda_2)\varepsilon^*_\mu(p_3,\lambda_3)\gamma^\mu S_N(p^{*2}_{2f})u(p_b,\lambda_b)g_{\omega NN}F_{\omega N^*N}(p^{*2}_{2f})F_{\mathbb{P}NN^*}(p^{*2}_{2f})$$
$$\times is_{ab}C^{NN}_{\mathbb{P}}\left(\frac{s_{ab}}{s_0}\right)^{\alpha_{\mathbb{P}}(t_1)-1}\exp\left(\frac{B^{NN}_{\mathbb{P}}t_1}{2}\right)\delta_{\lambda_1\lambda_a}, \tag{4.2}$$

$$\mathcal{M}^{(c)}_{\lambda_a\lambda_b\to\lambda_1\lambda_2\lambda_3} = \bar{u}(p_1,\lambda_1)S_N(p^{*2}_{1i})\varepsilon^*_\mu(p_3,\lambda_3)\gamma^\mu u(p_a,\lambda_a)g_{\omega NN}F_{\omega NN^*}(p^{*2}_{1i})F_{\mathbb{P}N^*N}(p^{*2}_{1i})$$
$$\times is_{12}C^{NN}_{\mathbb{P}}\left(\frac{s_{12}}{s_0}\right)^{\alpha_{\mathbb{P}}(t_2)-1}\left(\frac{s_{13}}{s_{\rm th}}\right)^{\alpha_N(p^{*2}_{1i})-1/2}\exp\left(\frac{B^{NN}_{\mathbb{P}}t_2}{2}\right)\delta_{\lambda_2\lambda_b}, \tag{4.3}$$

$$\mathcal{M}^{(d)}_{\lambda_a\lambda_b\to\lambda_1\lambda_2\lambda_3} = \bar{u}(p_2,\lambda_2)S_N(p^{*2}_{2i})\varepsilon^*_\mu(p_3,\lambda_3)\gamma^\mu u(p_b,\lambda_b)g_{\omega NN}F_{\omega NN^*}(p^{*2}_{2i})F_{\mathbb{P}N^*N}(p^{*2}_{2i})$$
$$\times is_{12}C^{NN}_{\mathbb{P}}\left(\frac{s_{12}}{s_0}\right)^{\alpha_{\mathbb{P}}(t_1)-1}\left(\frac{s_{23}}{s_{th}}\right)^{\alpha_N(p^{*2}_{2i})-1/2}\exp\left(\frac{B^{NN}_{\mathbb{P}}t_1}{2}\right)\delta_{\lambda_1\lambda_a}. \tag{4.4}$$

The diagrams for the interaction with emitted ω meson:

$$\mathcal{M}^{(e)}_{\lambda_a\lambda_b\to\lambda_1\lambda_2\lambda_3} = \bar{u}(p_1,\lambda_1)\gamma^\mu u(p_a,\lambda_a)S_{\mu\nu}(t_1)\varepsilon^{\nu*}(p_3,\lambda_3)g_{\omega NN}F_{\omega^*NN}(t_1)F_{\mathbb{P}\omega^*\omega}(t_1)$$
$$\times is_{23}C^{\omega N}_{\mathbb{P}}\left(\frac{s_{23}}{s_0}\right)^{\alpha_{\mathbb{P}}(t_2)-1}\left(\frac{s_{13}}{s_{\rm th}}\right)^{\alpha_\omega(t_1)-1}\exp\left(\frac{B^{\omega N}_{\mathbb{P}}t_2}{2}\right)\delta_{\lambda_2\lambda_b}, \tag{4.5}$$

$$\mathcal{M}^{(f)}_{\lambda_a\lambda_b\to\lambda_1\lambda_2\lambda_3} = \bar{u}(p_2,\lambda_2)\gamma^\mu u(p_b,\lambda_b)S_{\mu\nu}(t_2)\varepsilon^{\nu*}(p_3,\lambda_3)g_{\omega NN}F_{\omega^*NN}(t_2)F_{\mathbb{P}\omega^*\omega}(t_2)$$
$$\times is_{13}C^{\omega N}_{\mathbb{P}}\left(\frac{s_{13}}{s_0}\right)^{\alpha_{\mathbb{P}}(t_1)-1}\left(\frac{s_{23}}{s_{\rm th}}\right)^{\alpha_\omega(t_2)-1}\exp\left(\frac{B^{\omega N}_{\mathbb{P}}t_1}{2}\right)\delta_{\lambda_1\lambda_a}, \tag{4.6}$$

where $s_0 = 1$ GeV^2 and $s_{th} = (m_N + m_\omega)^2$.

In the above equations $u(p_i,\lambda_i)$, $\bar{u}(p_f,\lambda_f) = u^\dagger(p_f,\lambda_f)\gamma^0$ are the Dirac spinors (normalized as $\bar{u}(p)u(p) = 2m_N$) of the initial and outgoing protons with the four-momentum p and the helicities λ. The propagators of nucleons and ω meson can be written as

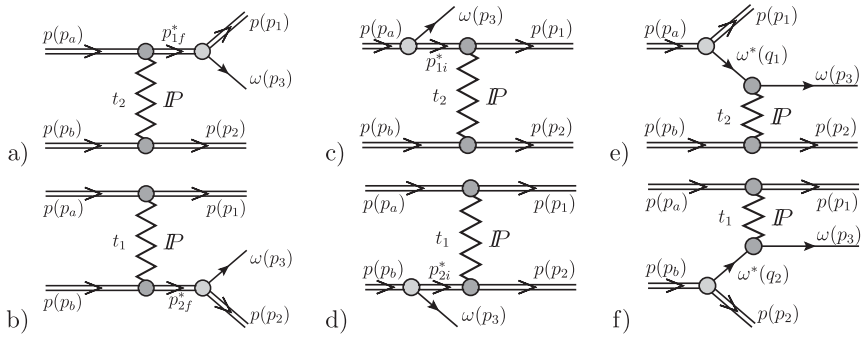

FIG. 6. Diagrams of the hadronic bremsstrahlung amplitudes included in the present paper.

$$S_N(p^{*2}_{1f,2f}) = \frac{i(p^*_{1f,2f_\nu}\gamma^\nu + m_N)}{p^{*2}_{1f,2f} - m_N^2},$$
$$S_N(p^{*2}_{1i,2i}) = \frac{i(p^*_{1i,2i_\nu}\gamma^\nu + m_N)}{p^{*2}_{1i,2i} - m_N^2}, \tag{4.7}$$
$$S_{\mu\nu}(t) = \frac{-g_{\mu\nu} + \frac{q_\mu q_\nu}{m_\omega^2}}{t - m_\omega^2},$$

where $t_{1,2} = (p_{a,b} - p_{1,2})^2 = q^2_{1,2}$, $p^{*2}_{1i,2i} = (p_{a,b} - p_3)^2$, $p^{*2}_{1f,2f} = (p_{1,2} + p_3)^2$ are the four-momenta squared of objects in the middle of diagrams and $s_{ij} = (p_i + p_j)^2$ are squared invariant masses of the (i, j) system.

The factor $g_{\omega NN}$ is the omega nucleons coupling constant. Different values have been used in the literature [22]. In our calculations the coupling constant is taken as $g^2_{\omega NN}/4\pi = 10$. A similar value was used in Refs. [16,18].

Using the known strength parameters for the NN and πN scattering fitted to the corresponding total cross sections (the Donnachie-Landshoff model [41]) we obtain $C^{NN}_{\mathbb{P}} = 21.7$ mb and $C^{\omega N}_{\mathbb{P}} = C^{\pi N}_{\mathbb{P}} = 13.63$ mb. The Pomeron/Reggeon trajectory determined from the elastic and total cross sections is taken in the linear approximation in t ($\alpha(t) = \alpha(0) + \alpha' t$):

$$\alpha_{\mathbb{P}}(t) = 1.0808 + 0.25t, \qquad \alpha_\omega(t) = 0.5 + 0.9t, \tag{4.8}$$

where the values of the intercept $\alpha(0)$ and the slope of the trajectory α' are also taken from the Donnachie-Landshoff model [41] for consistency. The slope parameter can be written as

$$B(s) = B_0 + 2\alpha'_{\mathbb{P}} \ln\left(\frac{s}{s_0}\right). \tag{4.9}$$

In our calculation we use B_0 $B^{\omega N}_{\mathbb{P}} = 5.5$ GeV^{-2} and $B^{NN}_{\mathbb{P}} = 9$ GeV^{-2}.

The extra factors $F_{\omega NN}$ and $F_{\mathbb{P}NN}$ (or $F_{\mathbb{P}\omega\omega}$) allow for modification when one of the nucleons or the ω meson is off its mass shell. We parametrize all the form factors in the following exponential form:

$$F_{\omega NN}(p^{*2}_{1f,2f}) = \exp\left(\frac{-(p^{*2}_{1f,2f} - m_N^2)}{\Lambda^2}\right),$$
$$F_{\mathbb{P}NN}(p^{*2}_{1f,2f}) = \exp\left(\frac{-(p^{*2}_{1f,2f} - m_N^2)}{\Lambda^2_{\mathbb{P}NN}}\right),$$
$$F_{\omega NN}(p^{*2}_{1i,2i}) = \exp\left(\frac{p^{*2}_{1i,2i} - m_N^2}{\Lambda^2}\right),$$
$$F_{\mathbb{P}NN}(p^{*2}_{1i,2i}) = \exp\left(\frac{p^{*2}_{1i,2i} - m_N^2}{\Lambda^2_{\mathbb{P}NN}}\right), \tag{4.10}$$
$$F_{\omega NN}(t_{1,2}) = \exp\left(\frac{t_{1,2} - m_\omega^2}{\Lambda^2}\right),$$
$$F_{\mathbb{P}\omega\omega}(t_{1,2}) = \exp\left(\frac{t_{1,2} - m_\omega^2}{\Lambda^2_{\mathbb{P}\omega\omega}}\right).$$

In general, the cutoff parameters are not known but could be fitted to the (normalized) experimental data. From our general experience in hadronic physics we expect $\Lambda \approx \Lambda_{\mathbb{P}NN} \approx \Lambda_{\mathbb{P}\omega\omega} = 1$ GeV. We shall discuss how the uncertainties of the form factors influence our final results.

Since the amplitudes given by formulas (4.5) and (4.6) are as if for ω meson exchanges they are corrected by the factors $(\frac{s_{ij}}{s_{th}})^{\alpha_\omega(t_{1,2})-1}$ to reproduce the high energy Regge dependence. We improve also the parametrization of the amplitudes (4.3) and (4.4), by the factors $(\frac{s_{ij}}{s_{th}})^{\alpha_N(p^{*2}_{1i,2i})-1/2}$, where we assume the nucleon trajectory $\alpha_N(p^{*2}_{1i,2i}) = -0.3 + \alpha'_N p^{*2}_{1i,2i}$, with $\alpha'_N = 0.9$ GeV^{-2}.

We have chosen a representation for the polarization vectors of the ω meson in the helicity states $\lambda_3 = 0, \pm 1$. The polarization vectors are parametrized, in a frame where $p = (E_3, p_3\cos\phi\sin\theta, p_3\sin\phi\sin\theta, p_3\cos\theta)$, as

$$\varepsilon(p_3, 0) = \frac{E_3}{m_\omega}\left(\frac{p_3}{E_3}, \cos\phi\sin\theta, \sin\phi\sin\theta, \cos\theta\right),$$
$$\varepsilon(p_3, \pm 1) = \frac{1}{\sqrt{2}}(0, i\sin\phi \mp \cos\theta\cos\phi, -i\cos\phi \mp \cos\theta\sin\phi, \pm\sin\theta). \tag{4.11}$$

It is easy to check that they fulfill the relation $p^\mu \varepsilon_\mu(p, \lambda) = 0$.

B. ω production as a diffractive excitation of the ωp-Fock state

The exclusive production of ω mesons in the fragmentation region of either proton can also be understood as a diffractive excitation of a two-body ωp-Fock state of the physical proton. This is best formalized by a Fock state decomposition of the protons light cone wave function in terms of meson-baryon Fock states. A comprehensive treatment of meson-cloud effects with applications to deep-inelastic scattering and baryon form factors within this framework has been developed in [40,42], for a review and references see [43]. For the problem at hand, we can write schematically

$$|p\rangle_{\rm phys} = \sqrt{Z}(|p\rangle_{\rm bare} + \int dz d^2\vec{k}_\perp \Psi_{\omega p}(z,\vec{k}_\perp)|p(1-z,-\vec{k}_\perp);\ \omega(z,\vec{k}_\perp)\rangle + \ldots). \tag{4.12}$$

Here, the bare proton state represents, for example, a three-quark core of the physical proton, and $\Psi_{\omega p}$ is the light cone wave function of the ωp-Fock state. The ω meson in the two-body Fock state carries a fraction z of light cone plus-momentum of the physical proton and transverse momentum $\vec{k}_\perp$; for simplicity helicity labels are suppressed. The invariant mass of the virtual ωp system is then given as

$$M^2_{\omega p} = \frac{\vec{k}^2_\perp + m^2_\omega}{z} + \frac{\vec{k}^2_\perp + m^2_N}{(1-z)}, \tag{4.13}$$

and enters the radial part of the wave function in terms of the ωNN-form factor

$$F_{\omega NN}(M^2_{\omega p}) = \exp\left(-\frac{M^2_{\omega p} - m^2_N}{2\Lambda^2_{\rm LC}}\right). \tag{4.14}$$

The parameter $\Lambda_{\rm LC}$ which controls the momentum distribution of ω mesons in the Fock state is taken as $\Lambda_{\rm LC} = 1.1$ GeV [40].

In accordance with the classic Good-Walker formalism [44], diffractive excitation of the ωp state now occurs because interactions of the bare proton and the two-body ωN state differ. We can write the ωp scattering state as

$$|\omega p\rangle_{\rm scatt} = (\hat{S}_{\omega p} - \hat{S}_p)|\omega p\rangle, \tag{4.15}$$

where $\hat{S}_{\omega p}$ and $\hat{S}_p$ are the elastic scattering matrices for the ωp and p interactions with the target. Assuming that the S matrix of the two-body state factorizes, $\hat{S}_{\omega p} = \hat{S}_\omega \hat{S}_p$, one can show that Eq. (4.15) generates precisely the diagrams a), c), e) of Fig. 6. Diagrams b), d), f) can be obtained by an obvious symmetrization. In the practical evaluation, these diagrams will give similar expressions in momentum space as the ones obtained in the Reggeized field theory model (the "standard approach" discussed above), modulo the absence of Regge-factors and the careful replacement of all ωNN-form factors by their light cone counterparts given in Eq. (4.14).

Notice that this description of diffractive dissociation, which treats the ω meson as a nonperturbative parton of the proton has a good physical motivation only in the fragmentation region of the proton (s). When the ω meson is produced in the central rapidity domain, the Reggeization of the crossed channel exchanges must be taken into account. For Reggeon exchanges however the light cone wave function formalism described above is ill defined [45]. Therefore, for a description of midrapidity ω production, one would have to add the Reggeized ω exchange. We do not do this here, as the final result would not differ much from the Reggeized field theory diagrams (the "standard approach"). At rapidities close to the proton fragmentation region the difference between the "standard approach" and the light cone wave function treatment can serve as an indicator for the model dependence of our predictions for this particular soft process.

Finally let us note, that at the high energies of interest the deviation from factorization

$$\delta\hat{S} = \hat{S}_{\omega p} - \hat{S}_\omega \hat{S}_p, \tag{4.16}$$

is quantified by the shadowing or absorption correction to which we now turn.

C. Absorption effects

The absorption effect for the hadronic bremsstrahlung contributions requires a short comment. Since in practice for the Pomeron exchanges in diagrams a)–d) we use phenomenological interactions which effectively describe the total and elastic data, an additional use of absorption would be a double counting. This is not the case for diagrams e) and f) where the interaction is between ω meson and proton. Consequently in the latter case we include an absorption effect in full analogy to that described in Sec. III A about photoproduction. This is illustrated in Fig. 7.

V. RESULTS

In the present section we present differential distributions for three different energies: $W = 200$ GeV (RHIC), $W = 1960$ GeV (Tevatron) and $W = 14$ TeV (LHC). This includes rapidity and transverse momentum of ω meson distributions as well as azimuthal correlations between outgoing protons.

In Fig. 8 we present differential cross sections $d\sigma/dW_{13}$ for the $pp \to pp\omega$ reaction at $W = 14$ TeV. We show

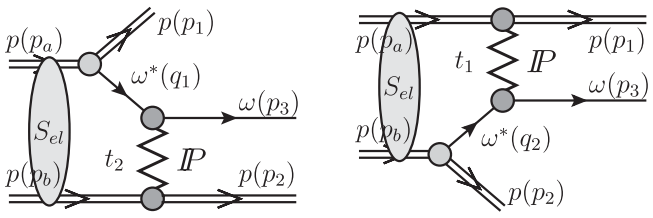

FIG. 7. The absorption effects included in the present paper for the ω bremsstrahlung.

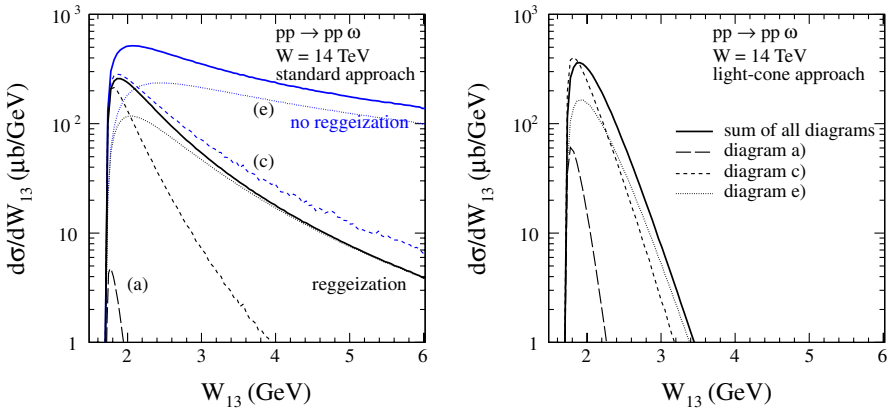

FIG. 8 (color online). Differential cross sections $d\sigma/dW_{13}$ for the $pp \to pp\omega$ reaction at $W = 14$ TeV for the hadronic bremsstrahlung mechanisms. The left panel is for results with Mandelstam variable dependents ωNN form factors and with Reggeization included while the light cone approach correspond to the right panel. The thick solid line presents the result for the coherent sum of all amplitudes shown in Fig. 6.

results with Mandelstam variable dependent form factors (left panel), which we will call standard in the following, and with light cone form factors (right panel). In the left panel we show results for the standard spin-1/2 propagators in diagrams a) and c) as well as with Reggezaition [46]. The long dashed, dashed and dotted lines correspond to contributions from diagrams a), c) and e), respectively. The thick solid line presents the coherent sum of all amplitudes. The light cone form factors lead to much steeper dependence of the cross section on W_{13} (W_{23}) than the standard form factors. The Reggezaition leads to an extra damping of the large W_{13} (W_{23}) cross section.

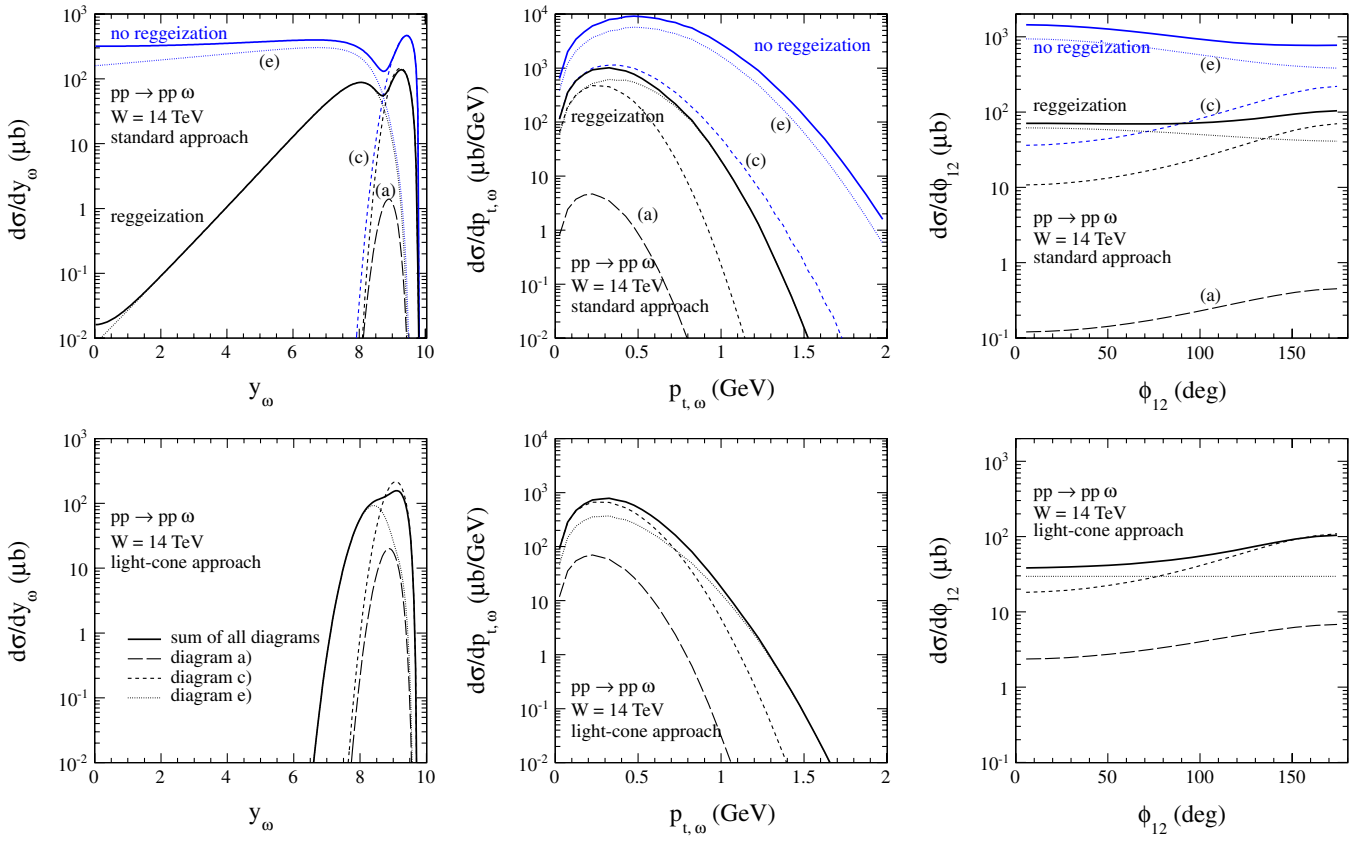

FIG. 9 (color online). Differential cross sections for the $pp \to pp\omega$ reaction at $W = 14$ TeV for the hadronic bremsstrahlung mechanisms. The upper panels are for results with Mandelstam variable dependents ωNN form factors and with Reggeization included while the light cone form factors correspond to the bottom panels. The thick solid line presents the cross sections for the coherent sum of all amplitudes shown in Fig. 6.

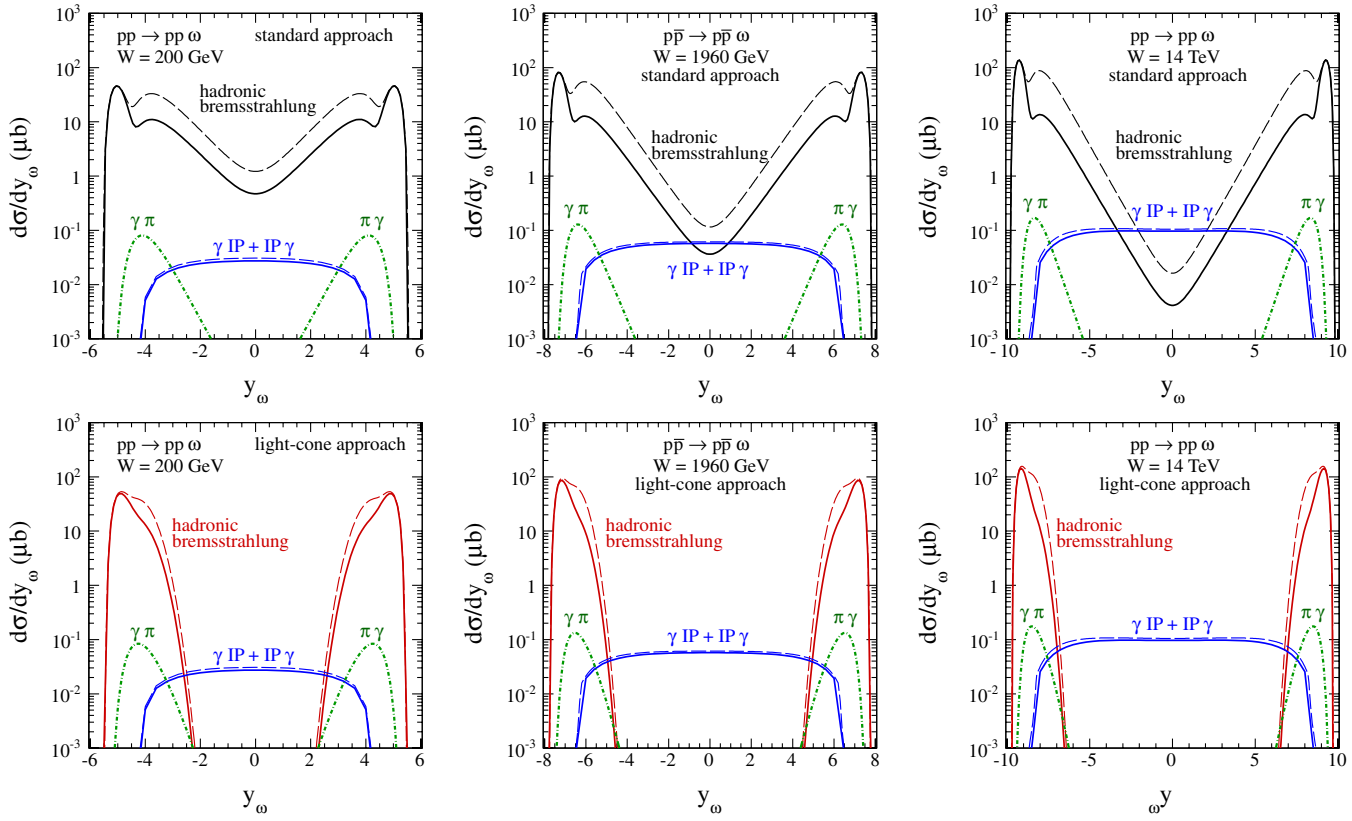

FIG. 10 (color online). Differential cross sections $d\sigma/dy_\omega$ for the $pp(\bar{p}) \to pp(\bar{p})\omega$ reaction at $W = 200$, 1960, 14000 GeV in the full rapidity range. The upper panels are for results with Mandelstam variable dependent ωNN form factors and with Reggeization included while the light cone form factors correspond to the bottom panels. In the latter case the Regge exchanges are evidently not included. The difference between the results with standard and light cone form factors illustrates theoretical uncertainties. The blue lines correspond to the QCD $\gamma\mathbb{P}$ and $\mathbb{P}\gamma$ mechanism. The green dash-dotted lines present the contribution of diagrams for the $\gamma\pi^0$ (left peak) and $\pi^0\gamma$ (right peak) exchanges. The dashed lines in the figures present the contributions without absorption, while the thick solid lines include the absorption.

In Fig. 9 we present the role of the form factors and Reggezaition for differential distributions in the ω meson rapidity and transverse momentum as well as for azimuthal angle correlation between outgoing protons. The distribution in rapidity is closely related to that for W_{13} (W_{23}). As seen from the middle panels the Reggezaition makes the distribution steeper in the ω meson transverse momentum.

In Fig. 10 we present rapidity distribution of the ω meson in the two approaches for different energies. In the first approach we use the standard ωNN form factors (upper panels) and in the second approach we use the light cone form factors (bottom panels) for the omega-nucleon-nucleon coupling. The distributions for the standard form factors extend more towards midrapidities. We show the $\gamma\mathbb{P}$ ($\mathbb{P}\gamma$), $\gamma\pi^0$ ($\pi^0\gamma$) as well as diffractive bremsstrahlung mechanisms. At "low" energy (RHIC) the discussed hadronic bremsstrahlung mechanisms dominate over the $\gamma\mathbb{P}$ and $\mathbb{P}\gamma$ ones. The cross section for the hadronic bremsstrahlung contribution is two-orders of magnitude bigger than that for the ($\gamma\mathbb{P}$, $\mathbb{P}\gamma$) contribution. The latter mechanism is known to be the dominant one for J/Ψ and Υ meson production [8,9]. A recent analysis at the Tevatron seems to confirm this claim [47]. Increasing the center-of-mass energy the hadronic bremsstrahlung components move to large rapidities. The $\gamma\pi^0$ (left peak) and the $\pi^0\gamma$ (right peak) components are separated. The separation in rapidity means also lack of interference effects which is very different compared to the $\gamma\mathbb{P}$ ($\mathbb{P}\gamma$) mechanism.[3] At LHC energy at midrapidities the photoproduction mechanisms with $\mathbb{P}$-exchange dominate over the hadronic bremsstrahlung ones. We predict a narrow plateau around $y \approx 0$ and a significant increase when going to large $|y|$. Experimental observation of the increase would confirm the bremsstrahlung mechanisms discussed here. Only at the highest LHC energy the region of very small rapidities is free of the hadronic bremsstrahlung contributions.

[3]The interference between the two mechanisms $\gamma\mathbb{P}$ and $\mathbb{P}\gamma$ is proportional to $e_1 e_2(\vec{p}_1 \cdot \vec{p}_2)$ and introduces a charge asymmetry as well as an angular correlations between the outgoing protons.

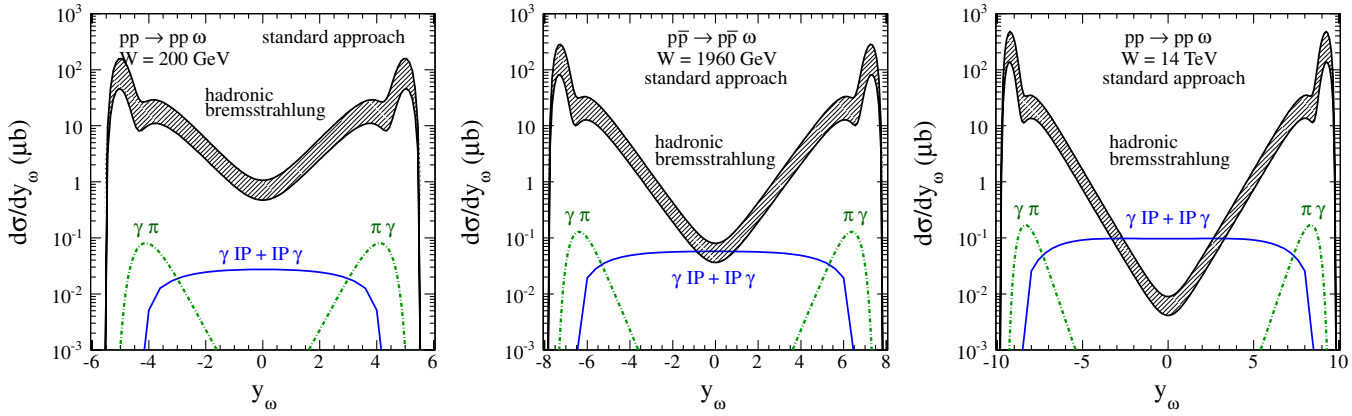

FIG. 11 (color online). Differential cross sections $d\sigma/dy_\omega$ for the $pp(\bar{p}) \to pp(\bar{p})\omega$ reaction at $W = 200$, 1960, 14000 GeV in the full rapidity range. The uncertainty band for the hadronic bremsstrahlung contributions related to the choice of the form factor parameter for $\Lambda = 1$ GeV (lower limit) and $\Lambda = 1.2$ GeV (upper limit).

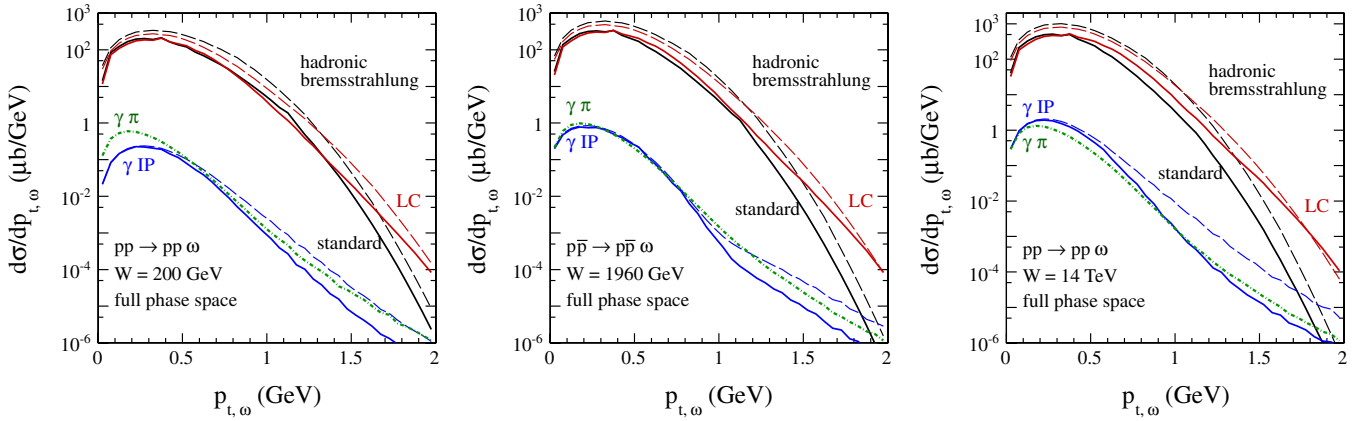

FIG. 12 (color online). Differential cross section $d\sigma/dp_t$ for the $pp(\bar{p}) \to pp(\bar{p})\omega$ reaction at $W = 200$, 1960, 14000 GeV in the full rapidity range. Here the Reggeized propagators of omega and nucleons are used. The dashed lines present the contribution without absorption, while the thick solid lines include the absorption.

How precise are our estimations of the bremsstrahlung contribution? In Fig. 11 we show the uncertainty band related to the choice of the form factor parameter. A similar uncertainty band can be expected due to the choice of the proton-proton-omega coupling constant. Our previous conservative estimation was a rather lower limit. While the hadronic bremsstrahlung contributions are subjected to rather large theoretical uncertainties. The $\gamma\mathbb{P}$ ($\mathbb{P}\gamma$) contributions are fairly precisely estimated. Deviations from the pQCD contribution at midrapidities may be caused by either the difficult to predict hadronic bremsstrahlung contributions or by the very interesting Pomeron-Odderon contributions. The rise of the cross section with increasing $|y|$ would be a clear signal of the hadronic bremsstrahlung contributions, while a sizeable deviation of the cross section normalization a potential signal of the Odderon exchange.

In Fig. 12 we show the distribution in the ω meson transverse momentum. In this case the integration is done over full range of meson rapidities. The dashed lines are for the Born level calculations while the thick lines include the effects of absorption. The hadronic bremsstrahlung contributions calculated in the light cone approach are similar to those in the standard approach. The distribution of the photon-Pomeron contribution for the $p\bar{p}$ scattering is somewhat different than that for the pp scattering. This is caused by different signs of the interference terms (different combination of electric charges). The distribution of the $\gamma\pi^0$ ($\pi^0\gamma$) contribution (green dash-dotted line) is very similar to that of the $\gamma\mathbb{P}$ ($\mathbb{P}\gamma$) contribution (blue lines).

Whether the $\gamma\pi^0$ mechanism can be identified requires further studies. What are other specific features of this mechanism ?

In Fig. 13 we show distribution in a relative azimuthal angle between outgoing protons. For the $\gamma\pi^0$ mechanism the maximum occurs at $\phi_{12} \approx \pi/2$ which is dictated by a specific tensorial coupling $\gamma\pi^0 \to \omega$. The azimuthal

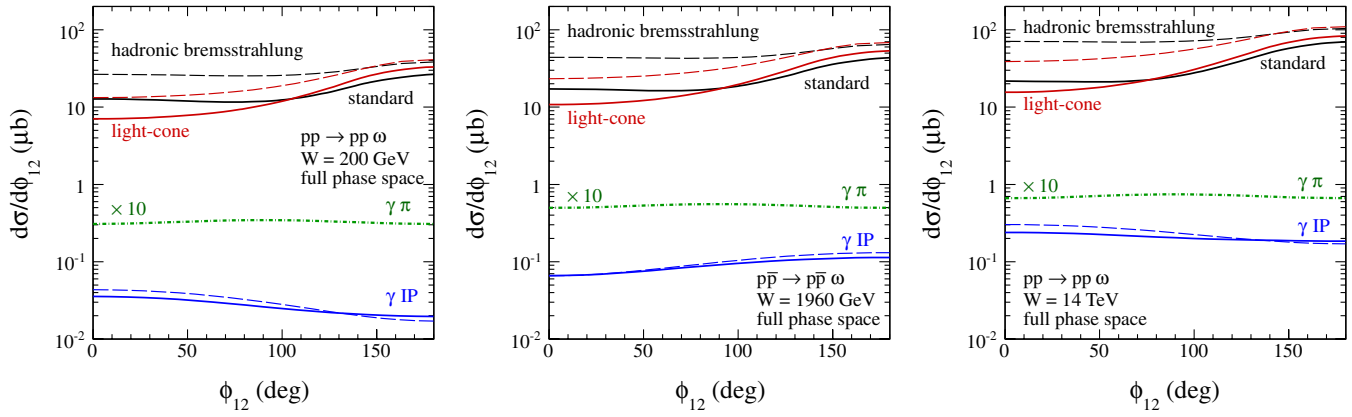

FIG. 13 (color online). Differential cross section $d\sigma/d\phi_{12}$ for the $pp(\bar{p}) \to pp(\bar{p})\omega$ reaction at $W = 200$, 1960, 14000 GeV in the full rapidity range. Here the Reggeized propagators of omega and nucleons are used. The dashed lines present the contribution without absorption, while the thick solid lines include the absorption.

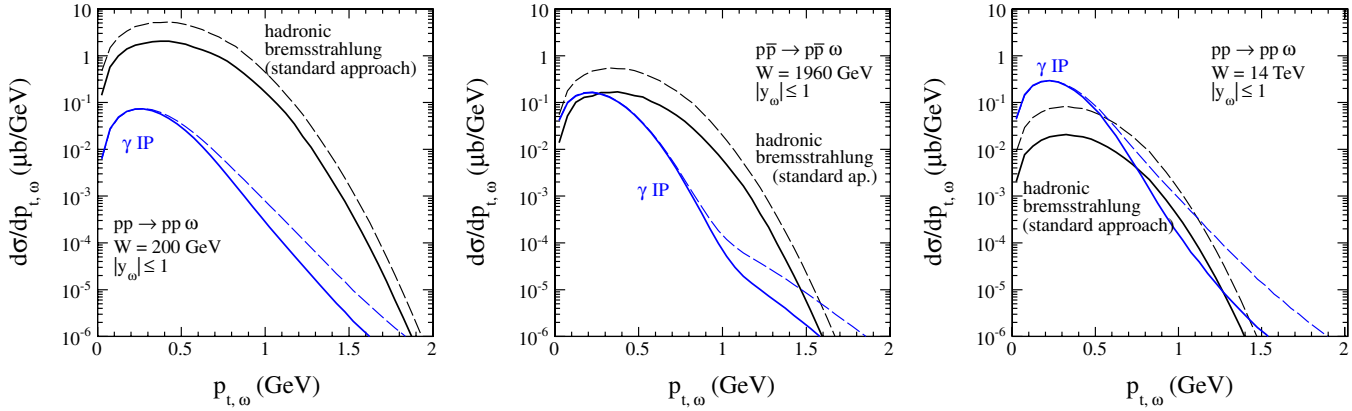

FIG. 14 (color online). Differential cross section $d\sigma/dp_t$ for the $pp(\bar{p}) \to pp(\bar{p})\omega$ reaction at $W = 200$, 1960, 14000 GeV for the limited rapidity range $-1 < y_\omega < 1$. Here the Reggeized propagators of omega and standard ωNN form factors are used. The dashed lines present the contribution without absorption, while the thick solid lines include the absorption.

distribution for the $\gamma\pi^0$ mechanism is very different than for the hadronic bremsstrahlung contributions which peak at $\phi_{12} = \pi$, especially for the light cone form factors. In principle, the azimuthal angle correlations could be used therefore to separate the different mechanisms. One can clearly see that the absorption effects (dashed lines) lead to extra decorrelation in azimuth compared to the results (thick solid lines). In Fig. 13 we show rapidity-integrated results. In general the azimuthal angle correlations are rapidity dependent. Quite different distributions for the $\gamma\mathbb{P}$ ($\mathbb{P}\gamma$) contribution have been predicted for the Tevatron and RHIC or LHC. The correlation function is for this mechanism caused totally by the interference of the $\gamma\mathbb{P}$ and $\mathbb{P}\gamma$ contributions (see [8]).

The distributions in the full (pseudo)rapidity range are rather theoretical and may be difficult to measure. One may expect that in practice only a limited range of (pseudo)rapidity around $y_\omega = 0$ will be available experimentally. Therefore, as an example, we have made an extra calculation for a limited rapidity range. In Fig. 14 we show transverse momentum distributions for $-1 < y_\omega < 1$. Here, as can be seen from Fig. 10, it is enough to include only the hadronic bremsstrahlung diagrams e) and f). In this case standard form factors are used only. Please note (see Fig. 10) that in the case of light cone form factors the hadronic bremsstrahlung mechanism does not contribute to the restricted rapidity region. For comparison we show the contributions of photoproduction mechanisms which are calculated fairly precisely as discussed before. This is very useful in the context of the searches for Odderon.

Finally in Fig. 15 we show angular correlations between outgoing protons for $-1 < y_\omega < 1$. In the case of light cone form factors only the photoproduction mechanism contributes. Testing such distributions together with

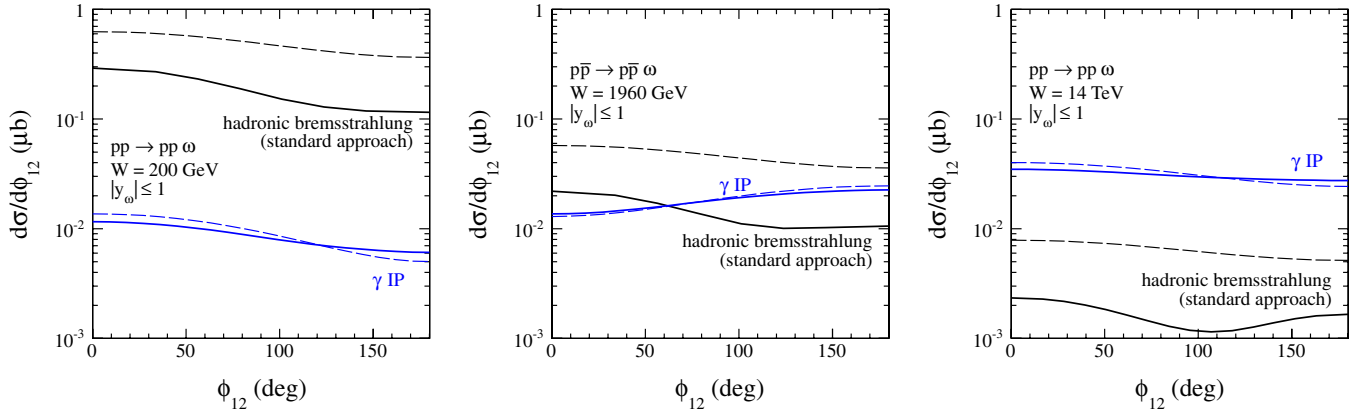

FIG. 15 (color online). Differential cross section $d\sigma/d\phi_{12}$ for the $pp(\bar{p}) \to pp(\bar{p})\omega$ reaction at $W = 200$, 1960, 14000 GeV for the limited rapidity range $-1 < y_\omega < 1$. Here the Reggeized propagators of omega and standard ωNN form factors are used. The dashed lines present the contribution without absorption, while the thick solid lines include the absorption.

rapidity distributions could provide therefore new information on the mysterious Odderon exchange.

VI. CONCLUSIONS

In this paper we have calculated the cross section for $\gamma p \to \omega p$ reaction at high energy within a QCD-inspired model. A good description of the HERA experimental data has been achieved, comparable as for the J/Ψ and ϕ mesons in our previous works. In the present paper the Gaussian wave function was used with parameters adjusted to reproduce the electronic decay width of the ω meson.

This model is used then to predict the cross sections for the $pp \to pp\omega$ and $p\bar{p} \to p\bar{p}\omega$ reactions at high energies for the first time in the literature. In contrast to the J/Ψ and ϕ exclusive production, in the case of the ω meson different hadronic bremsstrahlung processes are possible due to a large nonperturbative coupling of the ω meson to the nucleon. At high energy there is a class of diffractive bremsstrahlung processes never considered in the literature.

At low energies the hadronic bremsstrahlung contributions dominate over the photoproduction ones if the standard Mandelstam-dependent form factors are used. With increasing energy the hadronic bremsstrahlung contributions move in rapidity to the fragmentation regions. At high energies the photoproduction mechanisms dominate at midrapidities. We predict a short plateau at midrapidities due to the photoproduction mechanism and a significant increase towards fragmentation regions (large $|y_\omega|$) due to the ω bremsstrahlung. The identification of the increase would be a confirmation of the hadronic bremsstrahlung effects discussed here. However, this may be not simple experimentally. The precisely evaluated photoproduction mechanism constitutes a background for the Odderon exchange searches.

ACKNOWLEDGMENTS

This study was partially supported by the Polish Grant of MNiSW, Grant No. N202 249235 and Grant No. N202 322938.

[1] M. G. Albrow, T. D. Coughlin, and J. R. Forshaw, Prog. Part. Nucl. Phys. **65**, 149 (2010).
[2] R. S. Pasechnik, A. Szczurek, and O. V. Teryaev, Phys. Rev. D **78**, 014007 (2008); Phys. Lett. B **680**, 62 (2009); Phys. Rev. D **81**, 034024 (2010).
[3] I. P. Ivanov, N. N. Nikolaev, and A. A. Savin, Phys. Part. Nucl. **37**, 1 (2006).
[4] C. Marquet, R. B. Peschanski, and G. Soyez, Phys. Rev. D **76**, 034011 (2007).
[5] R. Fiore, L. L. Jenkovszky, V. K. Magas, S. Melis, and A. Prokudin, Phys. Rev. D **80**, 116001 (2009).
[6] I. V. Anikin, D. Yu. Ivanov, B. Pire, L. Szymanowski, and S. Wallon, Nucl. Phys. **B828**, 1 (2010).
[7] S. R. Klein and J. Nystrand, Phys. Rev. Lett. **92**, 142003 (2004).
[8] W. Schäfer and A. Szczurek, Phys. Rev. D **76**, 094014 (2007).
[9] A. Rybarska, W. Schäfer, and A. Szczurek, Phys. Lett. B **668**, 126 (2008).
[10] V. Rebyakova, M. Strikman, and M. Zhalov, Phys. Rev. D **81**, 031501 (2010).
[11] V. P. Goncalves and W. K. Sauter, arXiv:1004.1952.
[12] R. Enberg, J. R. Forshaw, L. Motyka, and G. Poludniowski, J. High Energy Phys. 09 (2003) 008;

G. G. Poludniowski, R. Enberg, J. R. Forshaw, and L. Motyka, J. High Energy Phys. 12 (**2003**) 002.
[13] A. Cisek, W. Schäfer, and A. Szczurek, Phys. Lett. B **690**, 168 (2010).
[14] A. A. Sibirtsev, Nucl. Phys. **A604**, 455 (1996).
[15] K. Nakayama, A. Szczurek, C. Hanhart, J. Haidenbauer, and J. Speth, Phys. Rev. C **57**, 1580 (1998); K. Tsushima and K. Nakayama, Phys. Rev. C **68**, 034612 (2003).
[16] N. Kaiser, Phys. Rev. C **60**, 057001 (1999).
[17] L. P. Kaptari and B. Kämpfer, Eur. Phys. J. A **23**, 291 (2004).
[18] K. Nakayama, Y. Oh, J. Haidenbauer, and T.-S. H. Lee, Phys. Lett. B **648**, 351 (2007).
[19] V. Flaminio *et al.*, Report No. CERN-HERA 84-10 1984; F. Balestra *et al.* (DISTO Collaboration), Phys. Rev. Lett. **81**, 4572 (1998); Phys. Rev. C **63**, 024004 (2001); F. Hibou *et al.*, Phys. Rev. Lett. **83**, 492 (1999); S. Barsov *et al.*, Eur. Phys. J. A **31**, 95 (2007); S. Abd El-Samad*et al.* (COSY-TOF Collaboration), Phys. Lett. B **522**, 16 (2001); M. Abdel-Bary *et al.* (COSY-TOF Collaboration), Phys. Lett. B **647**, 351 (2007); Eur. Phys. J. A **44**, 7 (2010).
[20] S. D. Drell and K. Hiida, Phys. Rev. Lett. **7**, 199 (1961); R. T. Deck, Phys. Rev. Lett. **13**, 169 (1964).
[21] A. B. Kaidalov, Phys. Rep. **50**, 157 (1979).
[22] R. Machleidt, K. Holinde, and Ch. Elster, Phys. Rep. **149**, 1 (1987); R. Machleidt, Adv. Nucl. Phys. **19**, 189 (1989).
[23] A. Schäfer, L. Mankiewicz, and O. Nachtmann, Phys. Lett. B **272**, 419 (1991).
[24] A. Bzdak, L. Motyka, L. Szymanowski, and J.-R. Cudell, Phys. Rev. D **75**, 094023 (2007).
[25] I. P. Ivanov, N. N. Nikolaev, and I. F. Ginzburg, *Proceedings of 9th International Workshop On Deep Inelastic Scattering (DIS 2001)*, edited by G. Bruni, G. Iacobucci, and R. Nania (World Scientific, Singapore, 2001); I. F. Ginzburg, I. P. Ivanov, and N. N. Nikolaev, Eur. Phys. J. direct C **5**, 02 (2003); Eur. Phys. J. direct C **32S1**, 23 (2003).
[26] Ph. Hägler, B. Pire, L. Szymanowski, and O. V. Teryaev, Phys. Lett. B **535**, 117 (2002); **540**, 324(E) (2002).
[27] P. Lebiedowicz and A. Szczurek, Phys. Rev. D **81**, 036003 (2010).
[28] M. Derrick *et al.* (ZEUS Collaboration), Z. Phys. C **73**, 73 (1996).
[29] M. Breitweg *et al.* (ZEUS Collaboration), Phys. Lett. B **487**, 273 (2000).
[30] I. P. Ivanov and N. N. Nikolaev, Phys. Rev. D **65**, 054004 (2002).
[31] A. Aktas *et al.* (H1 Collaboration), Eur. Phys. J. C **46**, 585 (2006).
[32] K. Nakamura *et al.* (Particle Data Group), J. Phys. G **37**, 075021 (2010).
[33] B. Friman and M. Soyeur, Nucl. Phys. **A600**, 477 (1996).
[34] Y. Oh, A. I. Titov, and T.-S. H. Lee, Phys. Rev. C **63**, 025201 (2001).
[35] G. Mennessier, S. Narison, and X.-G. Wang, Phys. Lett. B **696**, 40 (2011).
[36] T. E. O. Ericson, B. Loiseau, and A. W. Thomas, Phys. Rev. C **66**, 055206 (2002).
[37] J.-M. Laget, Phys. Lett. B **489**, 313 (2000).
[38] M. Williams *et al.* (CLAS Collaboration), Phys. Rev. C **80**, 065208 (2009).
[39] F. Abe *et al.* (CDF Collaboration), Phys. Rev. D **50**, 5518 (1994).
[40] H. Holtmann, A. Szczurek, and J. Speth, Nucl. Phys. **A596**, 631 (1996).
[41] A. Donnachie and P. V. Landshoff, Phys. Lett. B **296**, 227 (1992).
[42] Z. Dziembowski, H. Holtmann, A. Szczurek, and J. Speth, Ann. Phys. (N.Y.) **258**, 1 (1997).
[43] J. Speth and A. W. Thomas, Adv. Nucl. Phys. **24**, 83 (1997).
[44] M. L. Good and W. D. Walker, Phys. Rev. **120**, 1857 (1960).
[45] N. N. Nikolaev, W. Schäfer, A. Szczurek, and J. Speth, Phys. Rev. D **60**, 014004 (1999).
[46] J. K. Storrow, Phys. Rep. **103**, 317 (1984).
[47] T. Aaltonen *et al.* (CDF Collaboration), Phys. Rev. Lett. **102**, 242001 (2009).
[48] M. Derrick *et al.* (ZEUS Collaboration), Z. Phys. C **63**, 391 (1994).
[49] M. Derrick *et al.* (ZEUS Collaboration), Z. Phys. C **69**, 39 (1995).
[50] S. Aid *et al.* (H1 Collaboration), Nucl. Phys. **B468**, 3 (1996).
[51] M. Breitweg *et al.* (ZEUS Collaboration), Eur. Phys. J. C **2**, 247 (1998).
[52] C. Berger *et al.*, Phys. Lett. B **39**, 659 (1972); Y. Eisenberg *et al.* (SWT Collaboration), Phys. Rev. D **5**, 15 (1972); J. Park *et al.*, Nucl. Phys. **B36**, 404 (1972); J. Ballam *et al.* (SBT Collaboration), Phys. Rev. D **5**, 545 (1972); **7**, 3150 (1973); G. E. Gladding *et al.*, Phys. Rev. D **8**, 3721 (1973); W. Struczinski *et al.*, Nucl. Phys. **B108**, 45 (1976); R. M. Egloff *et al.*, Phys. Rev. Lett. **43**, 657 (1979); D. Aston *et al.* (OMEGA Photon Collaboration), Nucl. Phys. **B209**, 56 (1982).
[53] H. R. Crouch *et al.*, Phys. Rev. **155**, 1468 (1967); R. Erbe *et al.* (ABBHHM Collaboration), Phys. Rev. **175**, 1669 (1968); M. Davier *et al.*, Phys. Rev. D **1**, 790 (1970); Y. Eisenberg *et al.* (SWT Collaboration), Phys. Rev. D **5**, 15 (1972); J. Ballam *et al.* (SBT Collaboration), Phys. Rev. D **7**, 3150 (1973); W. Struczinski *et al.*, Nucl. Phys. **B108**, 45 (1976); R. M. Egloff *et al.*, Phys. Rev. Lett. **43**, 1545 (1979); Phys. Rev. Lett. **44**, 690(E) (1980); A. M. Breakstone *et al.*, Phys. Rev. Lett. **47**, 1782 (1981); D. Aston *et al.*, Nucl. Phys. **B209**, 56 (1982); D. B. Barber *et al.* (LAMP2 Group), Z. Phys. C **26**, 343 (1984); M. Atkinson *et al.* (OMEGA Collaboration), Nucl. Phys. **B231**, 15 (1984); J. Busenitz *et al.*, Phys. Rev. D **40**, 1 (1989).